DETERMINATION OF ICE SHAPES AND THEIR EFFECT ON THE AERODYNAMIC CHARACTERISTICS FOR THE UNPROTECTED TAIL OF THE A 300 *

Dr.-Ing. Boris Laschka, Dipl.-Phys. Rudolf E. Jesse
Messerschmitt-Bölkow-Blohm GmbH
Munich, W. Germany

Abstract

The tail surfaces of the European Airbus A 300 are not equipped with a de-icing or anti-icing system. It could be shown by analysis and tests that, under maximum icing conditions defined in FAR 25, the aircraft remains completely safe, stable and controllable within its flight envelope.

This paper outlines the procedure applied to determine the ice accretion on the unprotected surfaces and its influence on the aerodynamic characteristics of the airplane. This comprises:

- investigation of the most severe icing conditions within the flight regime
- theoretical calculation and analysis of ice shapes based on impingement analysis
- icing wind tunnel tests
- establishing aerodynamic data with ice accretion

essential flying characteristics would be encountered. All these steps were performed for the A 300 and contributed successfully to its certification.

Figure 1. A 300 in Flight

I. Introduction

The European Airbus A 300 belongs to the new class of wide-body aircraft. It is designed for a capacity of 220 to 340 passengers, a maximum operating speed of M = 0,86 and a range of 1200 to 2200 nm. The first airplane was successfully introduced into service in April of this year.

Early in the development phase it was decided not to protect the tail surfaces by a de-icing or anti-icing system in order to save weight at the rear of the aircraft and to simplify systems design. In order to ensure airworthiness under all possible extreme icing conditions, thorough investigations, to guarantee full flight safety, sufficient flying qualities and controllability have been performed. These studies covered the theoretical and experimental determination of the amount of ice, ice build up, and shape and the resulting aerodynamic implications. In addition, flight tests with artificial ice shapes as well as under natural icing conditions have been conducted to ensure that no hazardous degradations of the

II. Flight Regimes of Maximum Icing

There exist two different metereological icing conditions called "maximum continuous" and "maximum intermittent". The first one which applies here generally yields to be biggest amount of ice collected when no anti-/de-icing system is available whereas the second one is decisive for appropriate sizing of an anti-/de-icing system. It can be shown easily that for most transport airplanes the severest icing within the flight envelope will be encountered during holding where usually the airplane by traffic control reasons is not allowed to change altitude or location arbitrarily to avoid icing regimes and where appreciable flight times have to be expected. This applies also to the A 300 for which the severe special requirement - set forth by the German and French aviation authorities - of 45 minutes flight under maximum continuous icing conditions without experiencing degradations of the essential flying characteristics to clear the aircraft without anti-/de-icing devices had to be fulfilled.

* These investigations have been performed by Deutsche Airbus GmbH (DA) and Messerschmitt-Bölkow-Blohm GmbH (MBB) under contract of DA.

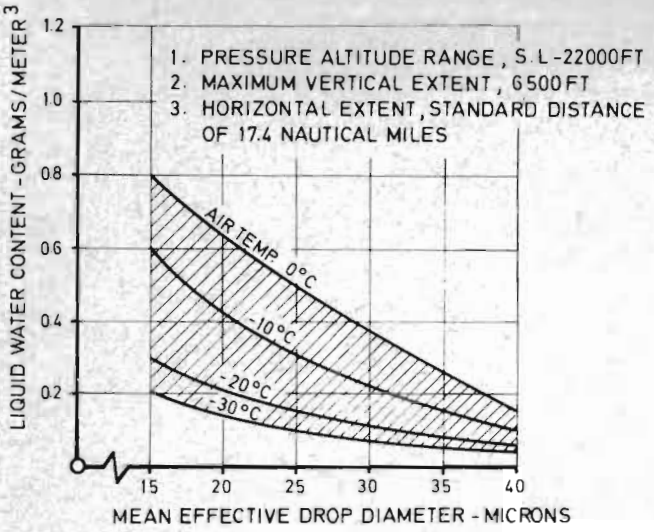

Continuous Maximum (Stratiform Clouds)
Atmospheric Icing Conditions

Figure 2a. Liquid Water Content Versus Mean Effective Drop Diameter

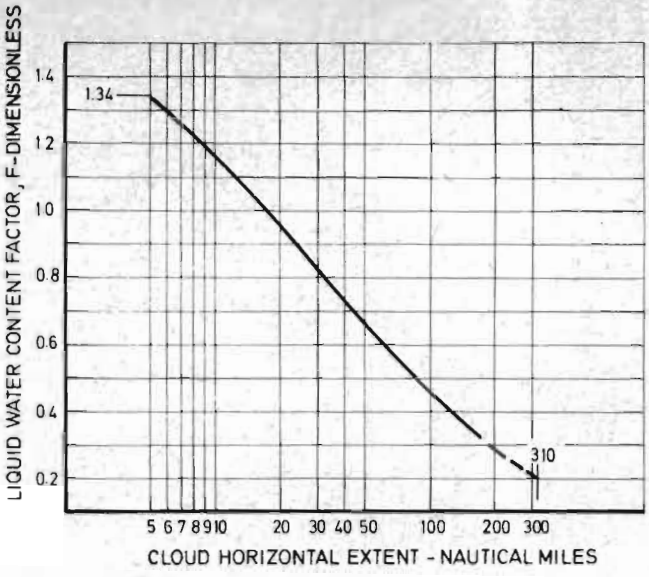

Continuous Maximum (Stratiform Clouds)
Atmospheric Icing Conditions

Figure 2c. Liquid Water Content **Versus** Cloud Horizontal Distance

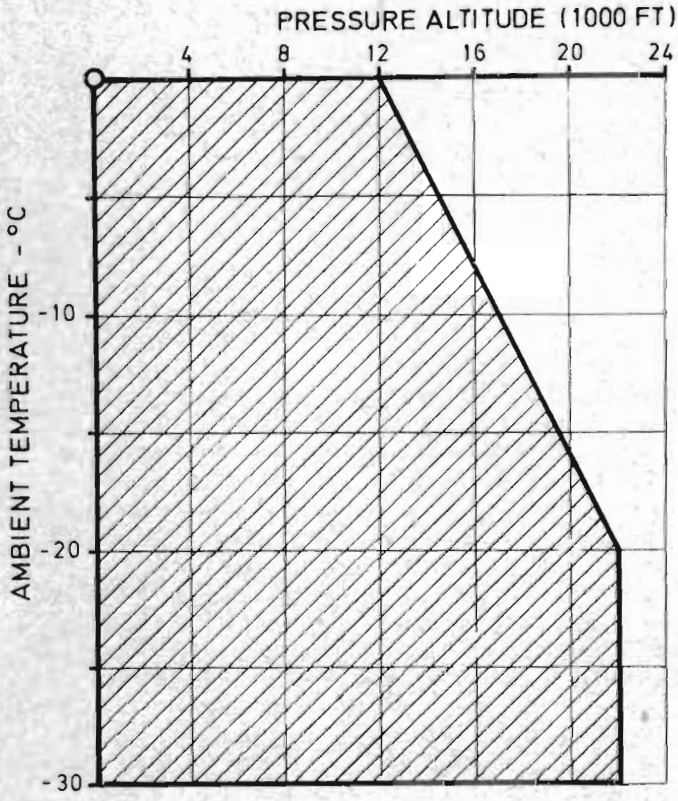

Continuous Maximum (Stratiform Clouds)
Atmospheric Icing Conditions

Figure 2b. Ambient Temperature Versus Pressure Altitude

From the statistical metereological data as given in FAR 25, App. C, [1], there exist a firm relationship between ambient temperature T, diameter of undercooled water droplets d and liquid water content LWC at all altitudes, fig. 2a and 2b. Liquid water content decreases with increasing flight distance, fig. 2c and decreases with ambient temperature fig. 2a, and temperature decreases with altitude, fig. 2b.

The average water captions per time unit is proportional to the liquid water content LWC, the true flight speed V and a caption factor K (depending on droplet diameter and wing flow).

$$\frac{dm_{water}}{dt} = K \cdot V \cdot LWC$$

Taking into account that the ambient temperature in the stagnation region of the tail surfaces has to be increased by $\Delta T = 0,2 \cdot T \cdot M^2 \cdot \cos^2\varphi$ (φ being tail l.e. sweep) one may easily conclude that for the A 300 biggest ice accretions have to be expected for holding at 230 kts CAS at ambient temperature from -5 to -10°C and at altitudes around 14 000 ft (fig. 3). Though cruise velocities are higher than at holding, no severe icing is to be expected, as because of the dynamic temperature increase only at very low temperatures at which LWC is small icing occurs. Certainly, at a later stage this first estimate has been substantiated by a more sophisticated impingement analysis.

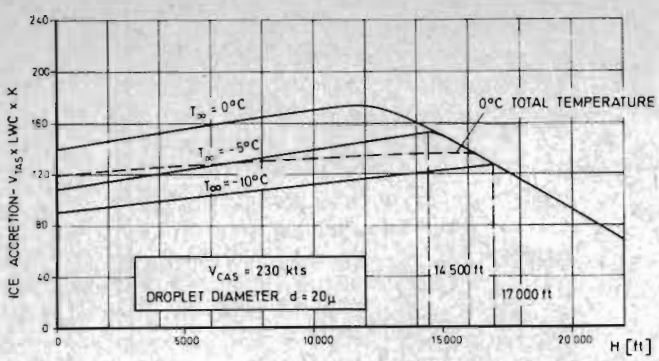

Figure 3. Average Amount of Ice Accretion Due to Flight Altitude and Air Temperature

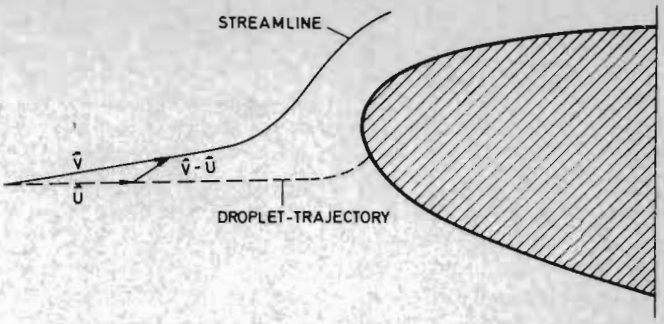

Figure 5. Vector Diagram for Droplet and Air Velocity

Impingement analysis also was mandatory to establish the influence of droplet size on total water caption. It cannot necessarily be concluded from fig. 2a that because of decrease of liquid water content with increasing droplet diameter the highest water caption goes with small droplets. Looking into the mechanism ruling the droplet trajectories one may find, that because of the inertial forces the bigger droplets tend to deviate more from the streamlines than the smaller ones in the vicinity of the leading edge.

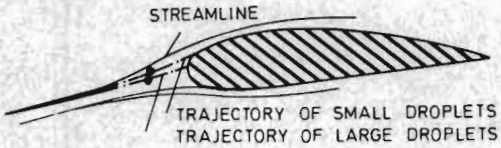

Figure 4. Deviation of Droplet Trajectories from Streamline Due to Droplet Diameter

The governing differential equation may easily be derived by the Newton law

$$\vec{K} = m \frac{d\vec{V}}{dt} \tag{1}$$

with m as mass of the droplet

$$m = \rho_{water} \frac{4}{3} \pi \left(\frac{d}{2}\right)^3 \tag{2}$$

and the only force $\vec{K}$ acting on the droplet given by its drag $\vec{D}$

$$\vec{K} = -\vec{D} = -c_D \cdot \pi \left(\frac{d}{2}\right)^2 \frac{\rho_{air}}{2} (\vec{U}-\vec{V}) \, |\vec{U}-\vec{V}| \tag{3}$$

From this the differential equation (1) can be transferred to

$$\frac{d\vec{V}}{dt} = \frac{3}{4} \frac{\rho_{air}}{\rho_{water}} \cdot c_D (Re_{droplet} = \frac{|\vec{V}-\vec{U}| \cdot d}{\nu_{air}}) \cdot \frac{(\vec{V}-\vec{U}) \, |\vec{V}-\vec{U}|}{d} \tag{4}$$

Generally the droplet Reynolds Number varies when the leading edge is approached, usually not exceeding a value of $Re_{droplet} = 20$, so that the Stoke's law for drag can be used with good approximation.

Equation (4) has been solved by classical difference methods [2] in combination with a panel method flow field calculation [3].

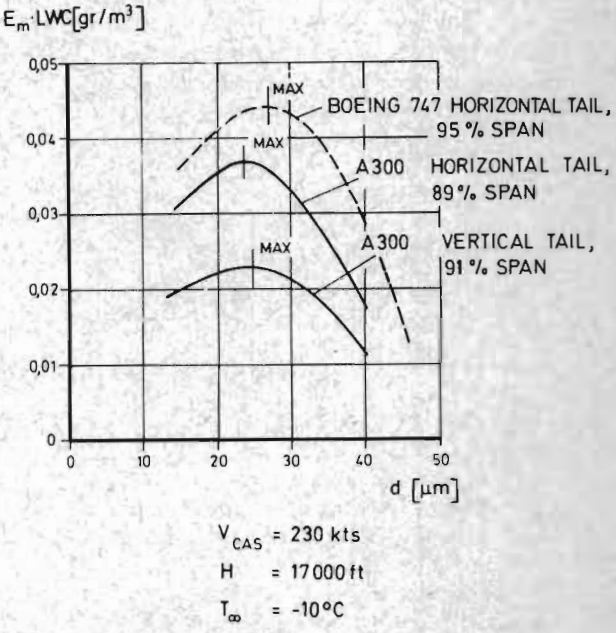

Figure 6. Water Caption Factor ($E_m \cdot LWC$) of Horizontal and Vertical Tail Versus Droplet Diameter

Analysis of the Airbus tail, fig. 6, revealed that the biggest water caption will be with droplets diameters between 20 μ and 28 μ both for the vertical as well as for the horizontal tail. Furthermore the calculations give evidence that ice accretion will be more severe for the horizontal tail. This is due to the fact that the horizontal tail has an absolute smaller leading edge radius than the vertical tail.

It is interesting to note that for the Boeing 747 also the horizontal tail showed to be the surface with the biggest water caption, but that the critical droplet size around 28 μ was somewhat bigger than at the Airbus [4]

III. Types of Ice Shapes

Of utmost importance for the alternation of the aerodynamic qualities is not only the amount of ice accretion but rather its shape.

Chordwise Ice Shapes

Generally, two types of ice shapes may be observed on airfoils (fig. 7).

- Rime ice results from low surface temperatures and low LWC. The water droplets freeze immediately after impinging on the leading edge of the airfoil and form a soft milky-white smooth and streamline ice shape around the leading edge. It does not occur when surface temperatures surpass -12°C. From the aerodynamic point of view these forms are not too bad, as they do not adversely affect lift- and drag characteristics of the airfoil and, sometimes, even result in an increase of lift (enlargement of airfoil-chord).

- Glaze ice (mushroom ice, double horn) forms at temperatures just below freezing point and high LWC.

  Glaze ice is normally formed at temperatures between 0°C and -8°C.

  At these temperatures water droplets do not freeze immediately after impingement but run first on the profile upward or downward from the stagnation point before they freeze when the temperature at the stagnation point is about 0°C or above, i.e. the so-called Ludlam limit is exceeded (freezing factor <1). The result is a deposit of ice with two horns like protrusions which is also called mushroom ice and normally is transparent and harder than rime ice.

  Such an ice shape is aerodynamically very unfavourable since the horn on the suction side spoils the flow and reduces the lift whereas the drag is increased.

- Intermittent ice is a mixture of rime ice and glaze ice having a form that lies between the two above types of ice. It consists of glaze ice at the front side and of rime ice at the rear. This form of ice is not so dangerous in aerodynamic respects than the glaze ice and develops between -6°C and -14°C.

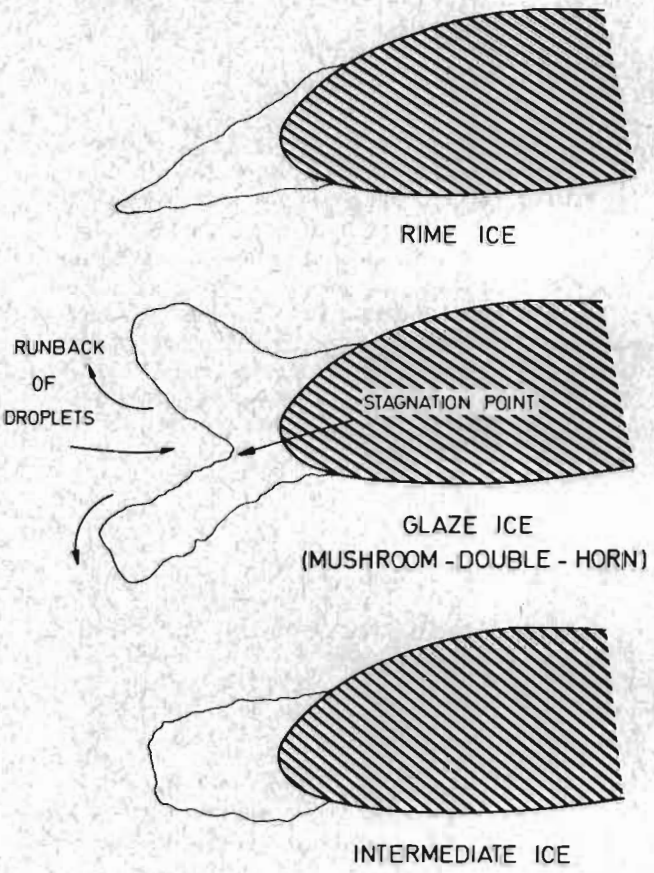

Figure 7. Types of Ice-Shapes

Naturally that mainly glaze ice need to be considered if aerodynamically critical icing is to be investigated.

Spanwise Ice Shapes for Swept Wings

On swept wings in addition to the just discussed chordwise ice shapes accretions with considerably segmented "notchings" similar to a "lobster tail" (see fig. 8) occur. The segments are curved in such a way, that their ends are bowed towards the wing tip.

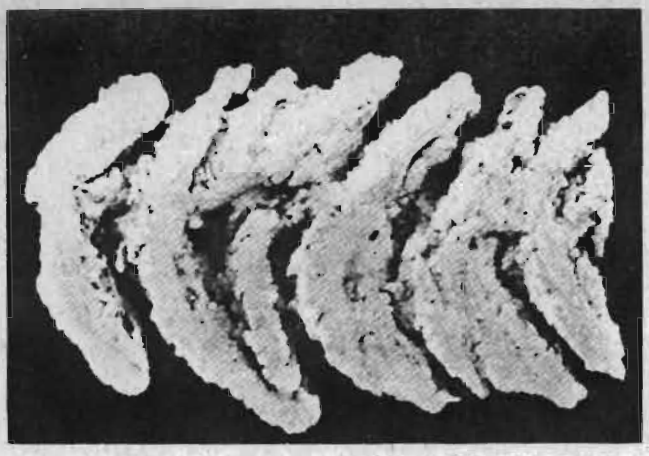

Figure 8. Lobstertail Cutting of a Typical A 300 Ice Shape

IV. Empirical Method for Determination of Ice Height

Computations assuming that

- all droplets impinging the contour freeze immediately
- breaking-off of ice deposits is neglected

do not show the mushroom shape. Such a calculation always predict ice heights considerably in excess of the real ones. Nevertheless, empirical methods are available, from which mushroom ice shapes may be derived. This method makes extensively use of measured upper horn lengths, h_{US}, lower horn length h_{LS} and thickness at the stagnation point h_{ST} for different yet similar profiles, which were plotted versus a quantity [2][4].

$$I = V_{TAS} \cdot t \cdot LWC \cdot E_M \cdot h^*/c$$

$$(kts \cdot min \cdot gr/m^3)$$

E_M = total droplet collection efficiency

h^*/c = ratio of profile thicknesses

A thus determined ice height at the horizontal tail of the A 300 is plotted versus span in fig. 9 for a selected case and then compared with B 747. In principle, ice height decreases with increasing profile thickness or - what is tantamount - for constant thickness ratios with increasing profile chord.

Almost the same ice height is found at the tip for both horizontal tails yet a different decrease of height toward the fuselage due to differences in airfoil thickness.

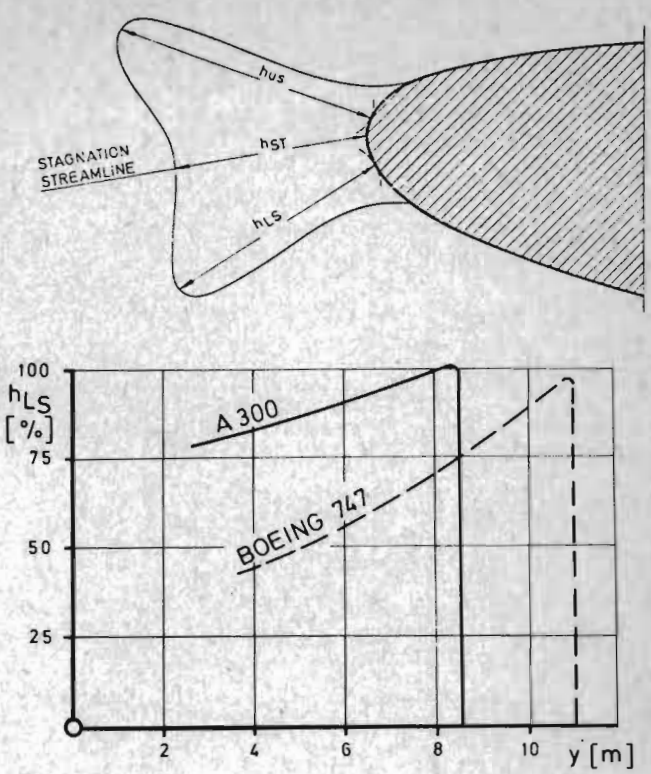

t = 30 min

H = 15000 ft

d = 15 µ

Figure 9. Spanwise Ice Heights for Horizontal Tail

V. Experimental Determination of Ice Shapes

It is obvious that the highly three-dimensional structure of the ice deposites as given by the mushroom and lobster-tail shape is not theoretically predictable with sufficient reliability whereas prediction of the total captured ice can well be done.

Therefore the above given caculation procedure was complemented by experiments in the icing tunnel of NASA, Lewis Center, Cleveland, Ohio.

Two horizontal tail-models of the A 300 (model 1 with constant profile thickness, model 2 was a portion of the horizontal tail in the original design configuration) were investigated [5]. Ice accretions have been determined by making plaster casts and photographs. The pressure distribution was likewise measured.

Test Results

The icing parameters e. g.

- ambient temperature $-5^\circ C \geq T_\infty \geq -10^\circ C$
- speed of flow $172 \leq V \leq 264$ mph

- volumetric diameter d of droplet
  $15\mu m \leq d \leq 25\mu m$
- concentration of liquid water
  $0,9 \leq LWC \leq 1.6\ gr/m^3$
- icing time $10 \leq t \leq 30$ minutes
- angle of attack $-4^o \leq \alpha \leq +2^o$

were varied within the above stated limits, in order to gain an insight into the significance of these parameters.

A study of the parameters [6], [7] yielded the following relationship:

1. Full repeatability was present (fig. 10)

α [°]	d [μ]	LWC [gr/m³]	T [°C]	CAS [mph]	t [min]
0	19	0.975	-5.5	230	21.6
0	19	0.975	-5	230	21.6

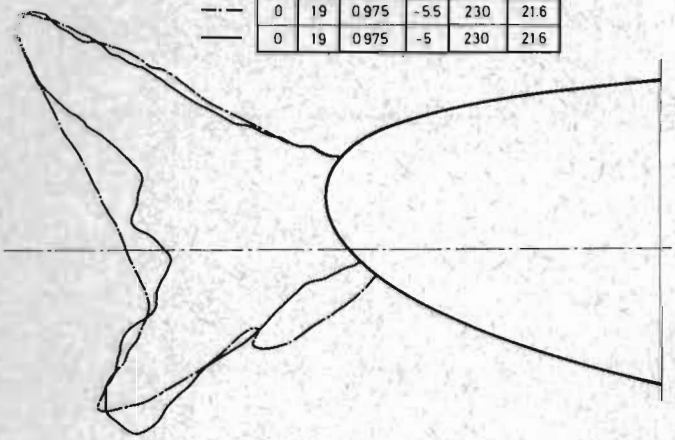

Figure 10. Repeatability

2. When varying LWC and time, while droplet diameter, velocity and temperature are kept constant one obtains the same ice shapes for all LWC · t = const. (see fig. 11).

α [°]	d [μ]	LWC [gr/m³]	T [°C]	CAS [mph]	t [min]
0	16	1.40	-5	184	14.2
0	16	1.30	-5	184	15.4
0	16	1.10	-5	184	18.2
0	16	0.90	-5	184	22.2

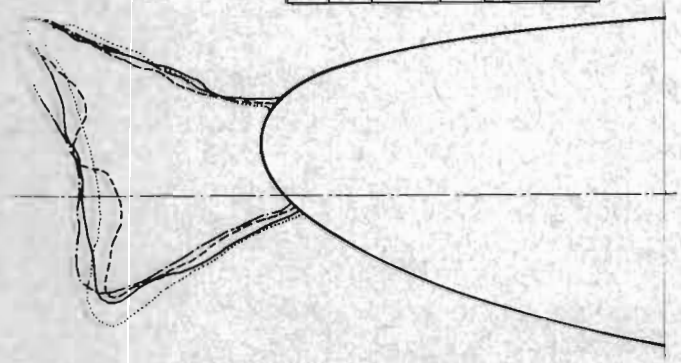

Figure 11. Effect of LWC x t = const.

3. If time varied with the same conditions, ice height will be approximately proportional to the time period of icing, while impingement limits are independent of time (see fig. 12). A slight nonlinear increase with time could be observed for already big ice accretions, which may be contributed to the increase of capture area with time.

α [°]	d [μ]	LWC [gr/m³]	T [°C]	CAS [mph]	t [min]
0	16	1.15	-5	192	10
0	16	1.15	-5	192	20
0	16	1.15	-5	192	25
0	16	1.15	-5	192	30

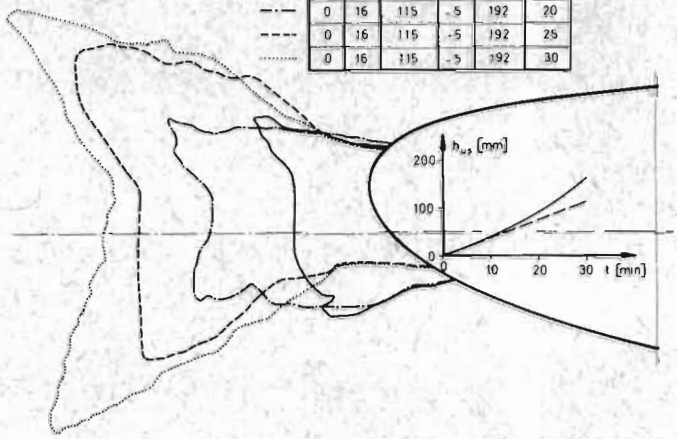

Figure 12. Effect of Icing-Duration

4. If velocity and time are simultaneously varied at constant LWC almost identical ice heights, yet different impingement limits and different horn configurations will be obtained on the condition V · t = const. (refer to fig. 13).

α [°]	d [μ]	LWC [gr/m³]	T [°C]	CAS [mph]	t [min]
0	20	1.20	-5	264.7	13
0	20	1.20	-5	242	14.3
0	20	1.20	-5	207	16.7
0	20	1.20	-5	172.5	20

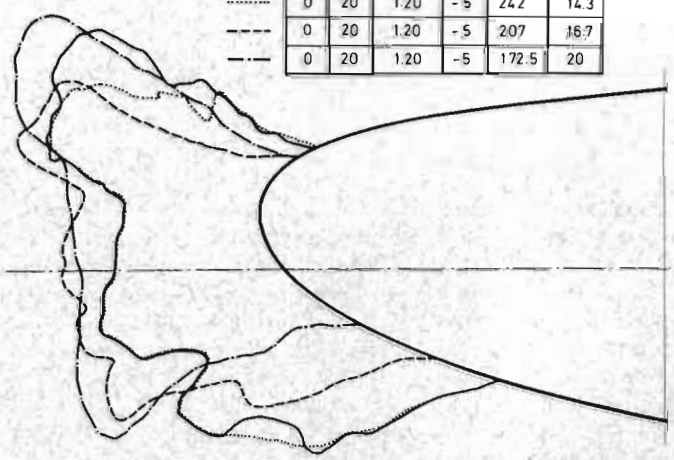

Figure 13. Effect of V x t = const.

5. If angle of attack is varied, different ice forms will be obtained; this condition implies migration of the stagnation point (see fig. 14).

From steps 2. through 4. it follows

ice height $\sim$ LWC · t · V = const.

ice shape $\sim$ LWC · t = const.

α [°]	d [μ]	LWC [gr/m³]	T [°C]	CAS [mph]	t [min]
2	19	0.975	-5	230	21.6
0	19	0.975	-5	230	21.6
-2	19	0.975	-5	230	21.6
-4	19	0.975	-5	230	21.6

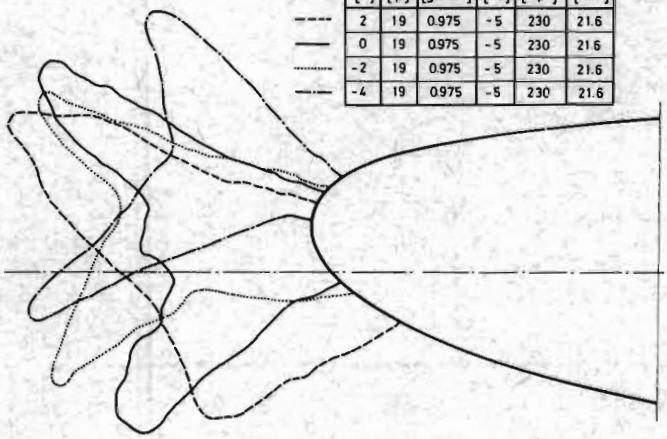

Figure 14. Effect of Angle of Attack

VI. Conversion of the Test Results to Real Flight Conditions

Conformity with actual flight conditions could not be achieved completely for some parameters like LWC and velocity. Moreover, since three-dimensional flow effects could not be exactly simulated, results had to be converted to actual flight conditions. Therefore, a special procedure [6][7] has been developed to deduce the ice accretion making use of both calculation and test results.

- First maximum ice accretion has been calculated and substantiated by experiment. The result was that the highest ice deposites occur near the tip of horizontal and vertical tail, the higher one on the horizontal tail. Its overall height was slightly below 3 inches. Therefore, this value has been adapted as a maximum. This is in accordance with observation of Boeing Company[4] that within 26 million flight hours on different airplanes no bigger accretions have occurred.

- Spanwise variation of the amount of ice has been assumed to be according to impingement analysis (see fig. 15). This has been substantiated for several tail surface sections by experimental results.

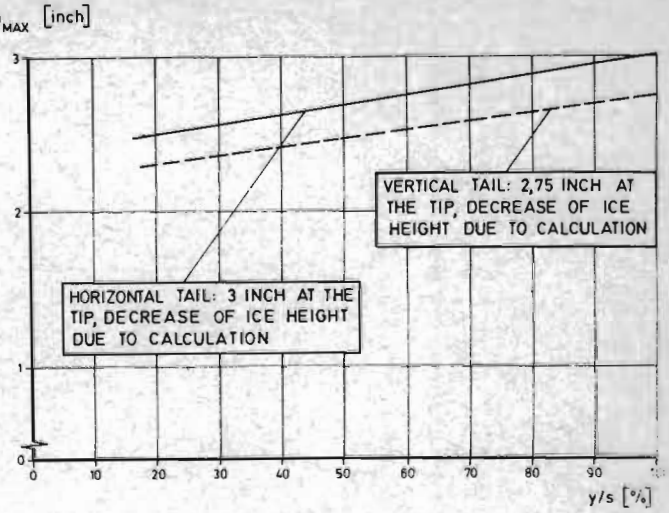

Figure 15. Maximum Ice Heights for Horizontal- and Vertical Tail (Spanwise)

- Chordwise and spanwise ice shapes have been fully taken according to the experimental shapes. Slight adjustments from test to flight conditions have been made using similarity laws [8]. Also, the angles of attack appertaining to the different actual flight cases were determined by adjusting the pressure distribution of the icing model to those of wind tunnel models, in order to provide aerodynamical equal conditions (refer to fig. 16). This procedure was performed separately for the upper and lower face.

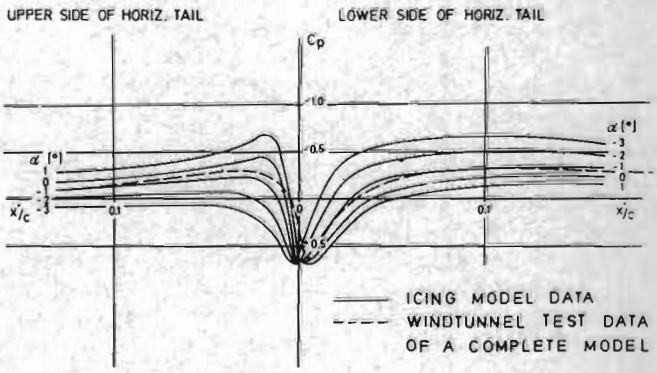

Figure 16. Pressure Distribution on Horizontal Tail Compared with Pressure Distribution for Flight Conditions

With this procedure, the most objectionable ice shapes have been evaluated and selected in order to be further investigated in wind tunnel and flight test. Fig. 17 depicts these ice shapes over the span of the horizontal tail. The corresponding notches may be seen in fig. 8.

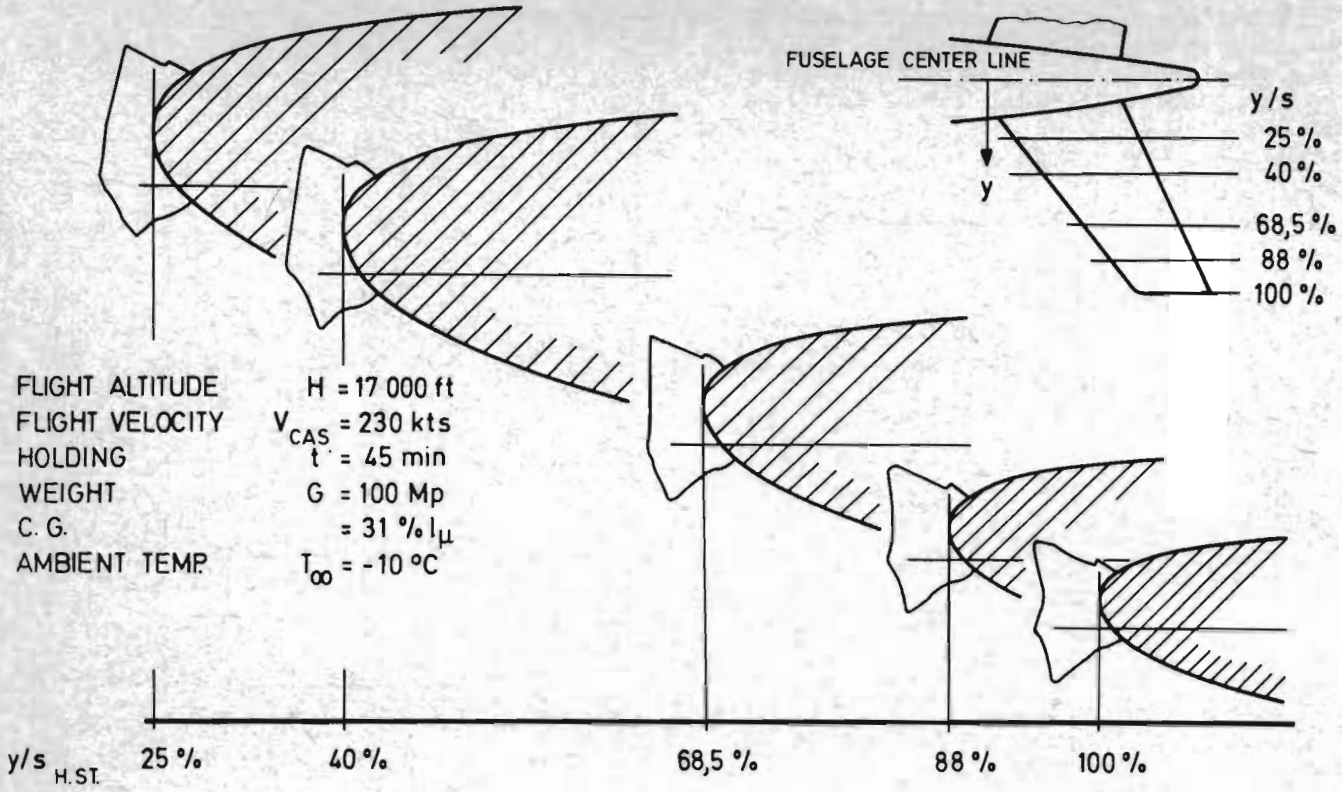

Figure 17. Ice-Shapes at Horizontal Tail

VII. Aerodynamic Investigations

Extensive wind tunnel testing with artificial ice accretions of the just described shape was performed in order to establish its influence on the most important aerodynamic data. These tests were done with complete models as well as pure tail models. The investigations included the determination of the influence of ice shapes, ice size, and notchings.

In fig. 18 the horizontal tail lift (c_L) versus angle of attack as determined with a tail model in the low speed wind tunnel of Braunschweig [9] shows that the deterioration effect of ice accretion sensitively depends of elevator angle. For high nose down moment elevator angles the loss in tail power at high negative angles of attack - what is equivalent to high negative tail settings - has shown to be not too serious. Maneouvers of interest in that range, such as stall recovery or go around where the pilot wants or has to increase the nose down moment remain nearly unaffected. On the other hand for high nose up moment elevator deflections, a loss in maximum negative tail lift can be observed which reduces the trimming and pulling capability at low speeds. Lift slope was associated only by minor changes. This was different to results on the vertical tail where an increase in lift slope according to the increase of fin area by the accretion was found.

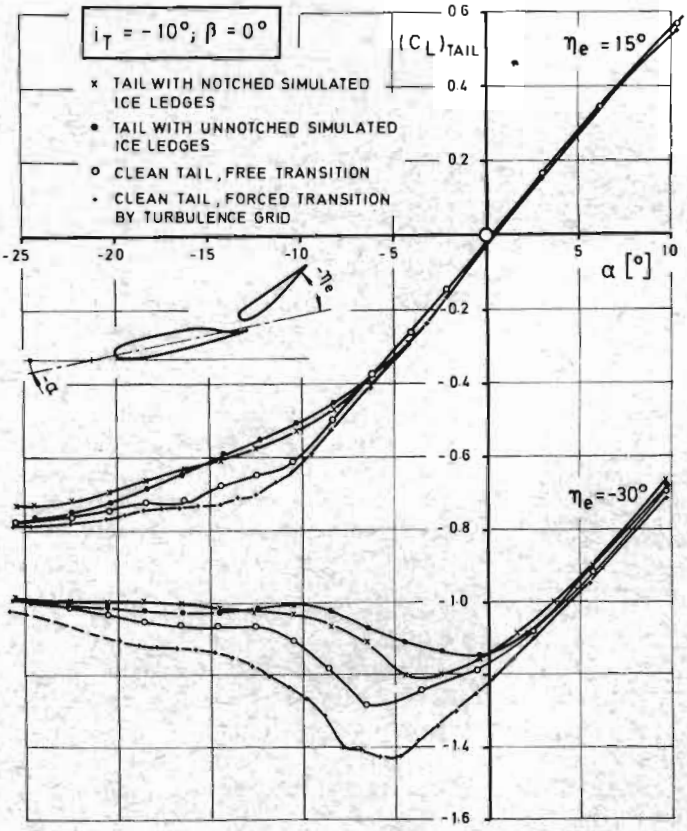

Figure 18. Effect of Ice Ledges on Tail Lift Characteristics

Ice accretions with notchings showed to have a favourable effect on stall onset as compared to results received without notchings. This is due to the effect that through the slots high energy flow is transported into the boundary layer or into the reattached bubbles, respectively, which exist immediately behind the ice protrusions. This may also be concluded from figure 19, where lift versus drag for the tail model has been plotted. Generally, the c_{D_O}-value is not affected very much by the ice but rather the drag due to high tail lift as occurs at operation with flaps and slats out.

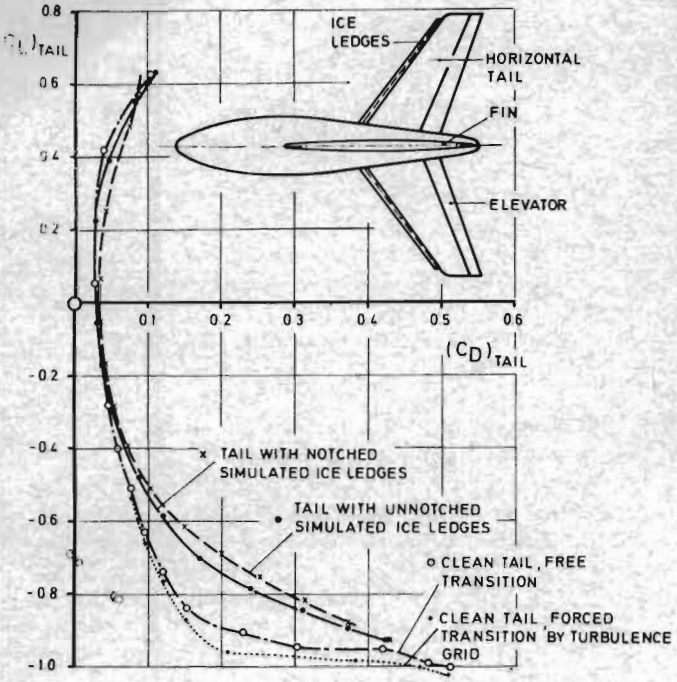

Figure 19. Effect of Ice Ledges on Tail Drag Characteristics

VIII. Flight Tests

Flight Tests with Simulated Ice

Simulator studies with aerodynamic data taking account for ice accretion showed that no degradating effects of any importance should be expected in flight. Nevertheless, before flight testing under natural icing conditions was released it was decided to have a flight program with simulated ice. The shapes were chosen according to paragraph VI, but because of the aerodynamic results of paragraph VII it was decided not to incorporate the lobster tail cutting. Consequently, these flight tests have been performed under more severe conditions than would be expected under natural icing.

The scope of investigation comprised

- forward and aft C. G. locations
- low speed tests in the clean, take-off and landing configuration, the latter including one engine failure, down to $V = V_S + 5 \div 6$ kts
- high speed tests up to V_{MO} and M = 0,835

At all these tests no instability or loss in control has occured, no sensible degradation of flying qualities was observed.

Fig. 20. Ice Ledge at Horizontal Tail

Flight Tests Under Natural Icing Conditions

Between March 26 and April 9, 1973, altogether 9 flights (36 flight hours) under natural icing conditions (5 flight hours) were performed with the prototype D02 of the A 300. One part of the tests was carried out over the Mediterranean Sea between the Northcoast of Tunesia, Sardinia and Southern Italy, the other part over the North Sea and the North-West of Germany [10].

The mean flight altitude was
$8.000 \leq H \leq 15.000$ ft at ambient
temperatures of $-3^{\circ}C \geq T_{\infty} \geq -16^{\circ}C$
and flight speeds of 140 kts $\leq V_{CAS} \leq$ 270 kts.
The liquid water content as determined during the flights, fluctuated between
$0.4\ g/m^3 \leq LWC \leq 1.0\ g/m^3$
the time periods of icing were
10 minutes $\leq t \leq$ 1 hour 20 minutes,
droplet diameter has not been recorded.

In order to sense ice formation and icing conditions and display it to the flight crew of the aircraft, two visual ice indicators (control rods; type CEV and Teddington) could directly be controlled from the cockpit. Two visible control rods at the nose box of the left hand side of the horizontal tail and on the lower side of the slat were filmed by a camera, and two ice detectors

(type REC - Rosemount-vibration-principle) were installed with quasi-stationary recording for LWC-determination and cockpit display used during entering icing conditions in flight (figure 21).

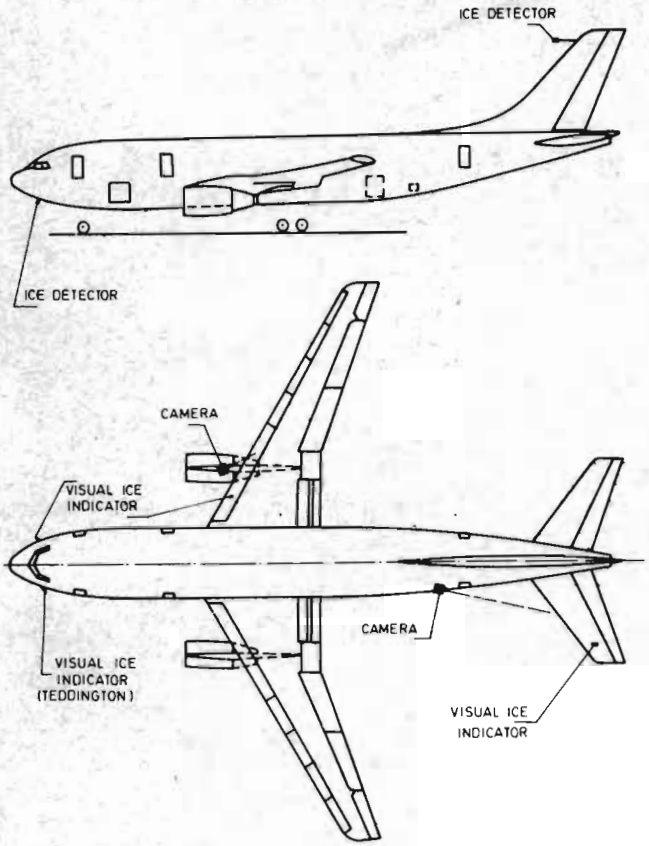

Figure 21. Installation of Cameras and Ice Detectors for Flight Tests

A photo of a specific deposit on the vertical tail may be seen in figure 22.

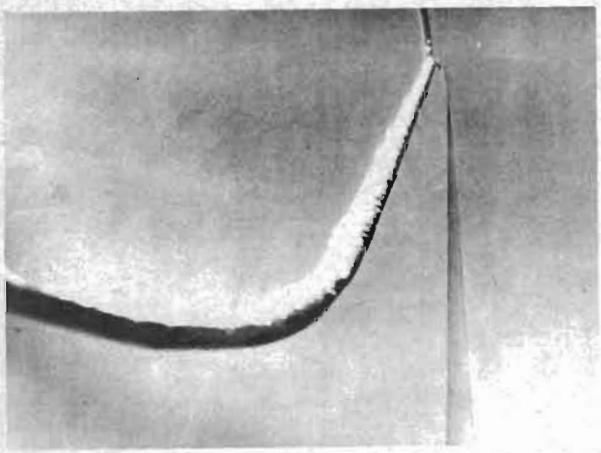

Figure 22. Ice Accretion on Vertical Stabilizer

In all cases the maximum assumed ice accretion was below three inches. Flight qualities of the aircraft during ice accretion were rated as very satisfactory by the pilots.

IX. References

(1) FAR Part 25, Appendix C
see also FAA-Advisory Circular No. 20-73

(2) W. Kraus: "Untersuchungen zur Leitwerks-vereisung der A 300-B, Teil 2: Theoretische Bestimmung der Eisformen und Eisverteilung"
Messerschmitt-Bölkow-Blohm Report
UFE 874-72, 6 June 1972

(3) W. Kraus: "Weiterentwicklung des Panel-verfahrens"
Messerschmitt-Bölkow-Blohm Report
UFE 1017, March 1973

(4) E. D. Dodson: "Determinations of ice shapes for unprotected B747 flight surface leading edge"
Boeing-Document No. D6-30-576, 1969

(5) H. Lück: "Vereisungsversuche am Höhenleit-werk der A 300-B im Eiskanal der NASA LRC in Cleveland Ohio"
Deutsche Airbus Report TB-EFW-6/71, 28 May 1971

(6) N. Kiesewetter: "Untersuchungen zur Leit-werksvereisung der A 300-B; Teil 1: Empirische Ermittlung der Eisformen"
Messerschmitt-Bölkow-Blohm Report
UFE 855-72, 28 February 1972

(7) R. E. Jesse: "Eisformen für die ungeschützten Leitwerke der A 300-B"
Messerschmitt-Bölkow-Blohm Report
UFE 865-72, 20 April 1972

(8) E. D. Dodson: "Scale Model Analogy for Icing Tunnel Testing"
Boeing-Document No. D6-7976, 1962

(9) P. Giese: "Windkanalmessungen am Airbus-Leitwerksmodell 108.3 Teil VII"
Deutsche Forschungsanstalt für Luft- und Raumfahrt e.V., Report No. IB-157-73 C3, 4 May 1973

(10) Airbus Industrie, Rapport d'Essais en Vol de Certification: "Justification de l'Avion en Atmosphère Givrante - Essais en Vol en Givrage Naturel Mésure"
Airbus Industrie Document PC/LG/MS AI/V n° 566/73, 17 September 1973